Monatshefte für Chemie - Chemical Monthly (2022) 153:1185–1196
https://doi.org/10.1007/s00706-022-02977-x

ORIGINAL PAPER

Evaluation of scandium sorption using modified Amberlite XAD-4 resin

Shaheeda Adonis[1] · **Tobie Oosthuysen**[1]

Received: 4 March 2022 / Accepted: 2 September 2022 / Published online: 5 October 2022

Abstract

Amberlite XAD-4 resin, impregnated with di(2-ethylhexyl)phosphoric acid (D2EHPA), was prepared as the adsorbent for this study. The loading capacity for the resin is 11.5 g of D2EHPA per gram of resin. Several parameters (adsorbent dosage, time, pH, initial metal concentration) were evaluated to investigate the adsorption capacity of the impregnated resin for Sc^{3+} from aqueous solutions. A maximum capacity of 0.035 mg Sc^{3+}/g of resin was achieved. The physical interaction of D2EHPA with the Amberlite XAD-4 resin was demonstrated using FT-IR. The adsorption data have been shown to fit well into the Langmuir isotherm. The pseudo-second-order model suitably describes the adsorption kinetics data, with a good correlation between the theoretical and experimental adsorption capacity values.

Graphical abstract

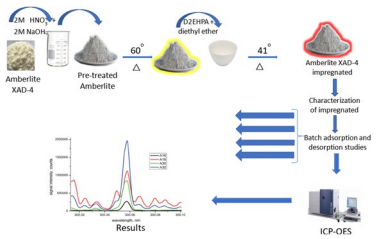

Keywords Adsorption · Extraction · IR Spectroscopy · Kinetics · Isotherms

Introduction

Lately, there has been adequate attention given to scandium owing to its rising demand. Scandium is a pioneering material, which has a wide application in the metallurgical, chemical, and electronic industries [1]. The growing interest in scandium and its compounds in chemical, optical, laser, and medical applications can be ascribed to its unique optical, mechanical, and electrical properties [2, 3, 31]. Scandium is also applied in solid oxide fuel cells (SOFC) [4], organic chemistry catalysts [5], high-intensity discharge lamps, and as an alloying agent [6]. However, the most significant application of scandium is attributed to solid oxide fuel cells (SOFC), which account for 90% of its total consumption and the remaining almost 10% of Sc is used in the Al-Sc alloy [30, 33]. In 2021, the principal uses of scandium were for SOFCs and aluminum–scandium alloys. Other uses for scandium included ceramics, electronics, lasers, lighting, and radioactive isotopes.

The increase in carbon emission from energy and mobility systems has been the cause of many environmental pollution problems [35]. The promotion and application of the new generation of SOFCs, that make use of scandium as a catalyst, can significantly reduce carbon emissions, working temperature, and power generation performance [34]. In view of the pressing need to decarbonize our energy and mobility systems globally, the future global demand for scandium can be expected to increase [36]. The prices estimated for scandium oxide in the United States in 2021

✉ Shaheeda Adonis
adoniss@cput.ac.za

[1] Department of Chemistry, Cape Peninsula University of Technology, Cape Town, South Africa

showed a significant decrease between 2020 and 2021 from 3.8 US$/g to 2.2 US$/g. This decrease is partly attributable to low-capacity utilization [28]. Scandium belongs to the group of rare-earth elements, which denotes the insufficiency of concentrated deposits occurring in trace amounts [7]. As a result, scandium is recovered as a by-product from residues and tailing wastes, often containing much higher concentrations of Fe, Al, and other metals. Owing to the low abundance of scandium, the main route of its production is as a by-product during the processing of ores which have a scandium content ranging between 20 and 50 ppm [9].

Potential sources of scandium pollution include the waste generated from the production of Al-Sc alloys [8], the vapor produced during the chlorination of titanium [35], acid mine drainage due to the processing from mineral deposits containing rare earth elements [33], scandium oxide production [34], and natural resources such as seawater and geothermal waters [39].

Information about the physiological and/or toxicological role of scandium is highly limited. The toxicokinetics and toxic dynamics of scandium depends on the form, the metal compound and the organisms' ability to store the element. Scandium poses hardly any risk to plants, whereas some research has indicated that scandium could possibly be carcinogenic. With long-term exposure, when scandium damps and gases are inhaled with air, it can cause lung embolisms [38]. Scandium can also be perilous for the liver when it accumulates in the human body.

The separation and purification of scandium from aqueous solutions are conventionally performed using precipitation, solvent extraction, and ion-exchange chromatography. The most significant drawbacks of these methods are the low scandium purity that yields from precipitation due to the co-precipitation of other metals present and the use of large amounts of organic reagents, sediment generation, and these methods inefficiency for low concentrations [7, 10, 11]. Ion-exchange chromatography displays high adsorption capacity and less complex operations. In addition, its maintenance costs are lower than those of solvent extraction [12, 13]. The application of ion-exchange chromatography to solutions with trace amounts of scandium contaminants is not advised due to resin performance being lost due to the impurities [14]. Despite the advantages of solvent extraction, it also has a few drawbacks, such as loss of extractant, especially for the organophosphorus extractants [15].

Many extractants have been investigated for separation of scandium, such as tributyl phosphate [17], ionic liquids [16], *N*-[*N*,*N*-di(2-ethylhexyl)aminocarbonylmethyl]glycine [7], and di(2-ethylhexyl)phosphoric acid (D2EHPA) [18, 32, 37]. D2EHPA impregnated XAD-7 resin was also used to investigate the purification of ^{89}Sr from an FBTR irradiated Yttria target [19]. The adsorption and desorption behavior of strontium from aqueous solutions was evaluated using an impregnated Amberlite XAD-4-D2EHPA resin [20].

In this study, the adsorption capacity of Amberlite XAD-4-di(2-ethylhexyl)phosphoric acid (D2EHPA) resin to separate scandium from aqueous solutions is evaluated, using solvent-impregnated resins. Solvent-impregnated resins (SIRs) are selected owing to their good advantages. SIRs involve incorporating the extractant (ligand) through physical impregnation into a given microporous polymeric support [24]. SIRs can selectively bind to specific metals owing to an organic functional group(s) impregnated into the support. SIRs thus have the combined advantage of ion exchange and solvent extraction [21, 22]. In addition, the suitable physical properties and chemically homogenous non-ionic structure of the Amberlite XAD resins make them promising sorbents for the preparation of solvent-impregnated resins using organophosphorus extractants [23].

Results and discussion

Impregnation

To evaluate the efficiency of the impregnation processes, the resin's loading capacity was determined by assessing the degree of D2EHPA loading onto the resin by contacting the resin with a series of solutions of different concentrations of D2EHPA. The loading capacity for each solution was calculated through titration with 0.1 M NaOH. As the volume of D2EHPA increased, the results showed a constant increase in loading capacity without a plateau. Since no plateau was reached, adsorption performance tests were conducted to evaluate the effect of loading ratios on the adsorption performances of the adsorbent for scandium. The loading capacity of the resin and the distribution coefficients of the adsorbent for the different loading ratios are illustrated in Fig. 1a, b, respectively.

The following equation was used to calculate the distribution coefficient:

$$K_{\mathrm{d}} \frac{\text{conc. of metal in resin}}{\text{conc. of metal in solution}} \times \frac{\text{cm}^3 \text{ of solution}}{\text{grams of resin}} \tag{1}$$

The maximum value for the distribution coefficient was observed at a volume of 12 cm^3 of extractant (loading capacity of 11.5 g D2EHPA/g XAD-4). Adsorption performance generally increases proportionally to the loading capacity. This deviation from the expected trend could be due to the leakage of the extractant from the SIR at higher loading. For this study, 12cm^3 of D2EHPA was used per 1 g of Amberlite XAD-4 resin.

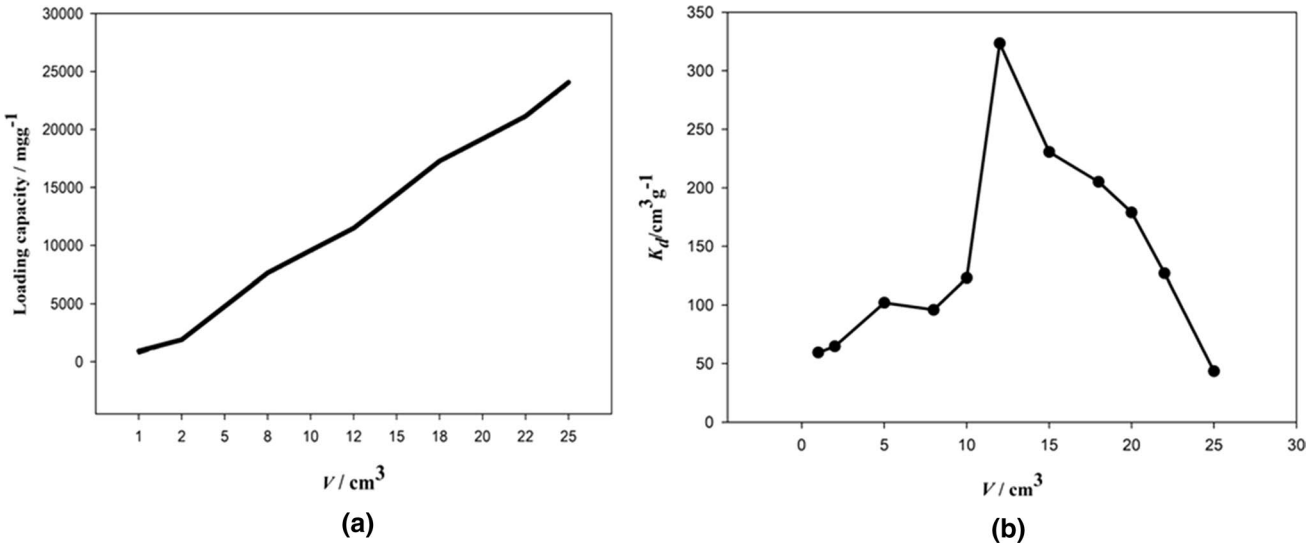

Fig. 1 **a** Loading capacity of resin and **b** distribution coefficient values at varying extractant volumes

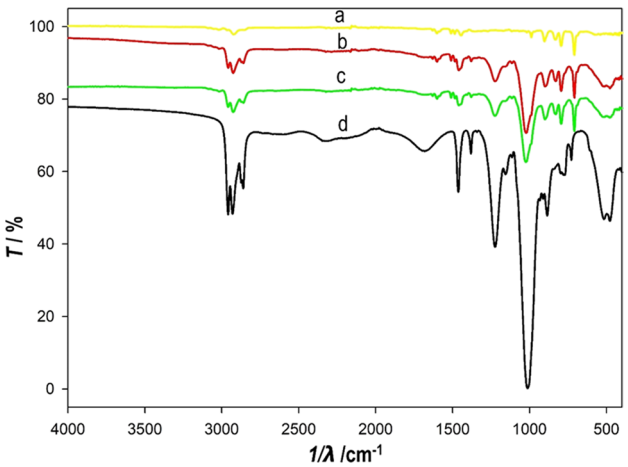

Fig. 2 FT-IR spectra of **a** Amberlite XAD-4, **b** XAD-4-D2EHPA, **c** XAD-4-D2EHPA-Sc, and **d** D2EHPA in the region 400–4000 cm^{-1}

Characterization of impregnated resin

The characterizations of the impregnated resin are presented from a comparative point of view using Fourier Transform Infra-Red (FT-IR) spectroscopy and Scanning Electron Microscopy (SEM).

FT-IR characterization of the Amberlite XAD-4, D2EHPA, and the D2EHPA impregnated XAD-4 resin

The FT-IR spectra of Amberlite XAD-4, D2EHPA, and the D2EHPA impregnated XAD-4 resins are represented in Fig. 2. Amberlite XAD-4 (Fig. 2a) is a polystyrene-based and nonpolar resin with aliphatic C-H stretching at 2923 cm^{-1}, C=C ring stretching at 1606, 1485, 1446 cm^{-1}, and the ring substitution at 903 cm^{-1}. The characteristic IR bands of neat D2EHPA (Fig. 2d) appear at 1224 cm^{-1} for the stretching vibrational band of the P=O bond, the P-O-C stretching vibration at 1012 cm^{-1}, and the P–OH vibration at 2323 cm^{-1}. Slight changes are observed in the P=O bond and the P–O–C stretching from 1224 cm^{-1} to 1225 cm^{-1} 1012 cm^{-1} to 1024 cm^{-1}, respectively, for the D2EHPA-XAD-4 impregnated resin (Fig. 2b). The shifts in wavenumbers could be an indication of the effective interaction between D2EHPA and Amberlite XAD-4 resin [24]. The FT-IR spectra of D2EHPA-XAD-4 impregnated resin loaded with scandium (Fig. 2c) show a reduction and shift in the P=O vibration from 1225 cm^{-1} to 1224 cm^{-1}, which indicates that the oxygen atom of P=O is involved in a complex formation with scandium. The P–O–C stretching vibration in the D2EHPA-XAD-4 impregnated resin shifts from 1024 cm^{-1} to 1021 cm^{-1} when scandium is loaded on the resin, indicating that the Sc^{3+} ions replace the H^+ ion of D2EHPA in solution as a result of the cation exchange process [24].

It can be noted that with the modification of XAD-4, the adsorbent peak at about 2923 cm^{-1} is less prominent in Fig. 2a compared to Fig. 2b–d. This may be the result of the C-H (CH_3) stretching for D2EHPA, indicating that the impregnation process was successful.

Scanning Electron Microscopy (SEM) characterization of the Amberlite XAD-4, D2EHPA, and the D2EHPA impregnated XAD-4 resin

Figure 3 represents the SEM images of Amberchrom XAD-4 before and after impregnation with D2EHPA. The SEM image for Amberlite XAD-4 (Fig. 3a) illustrates the

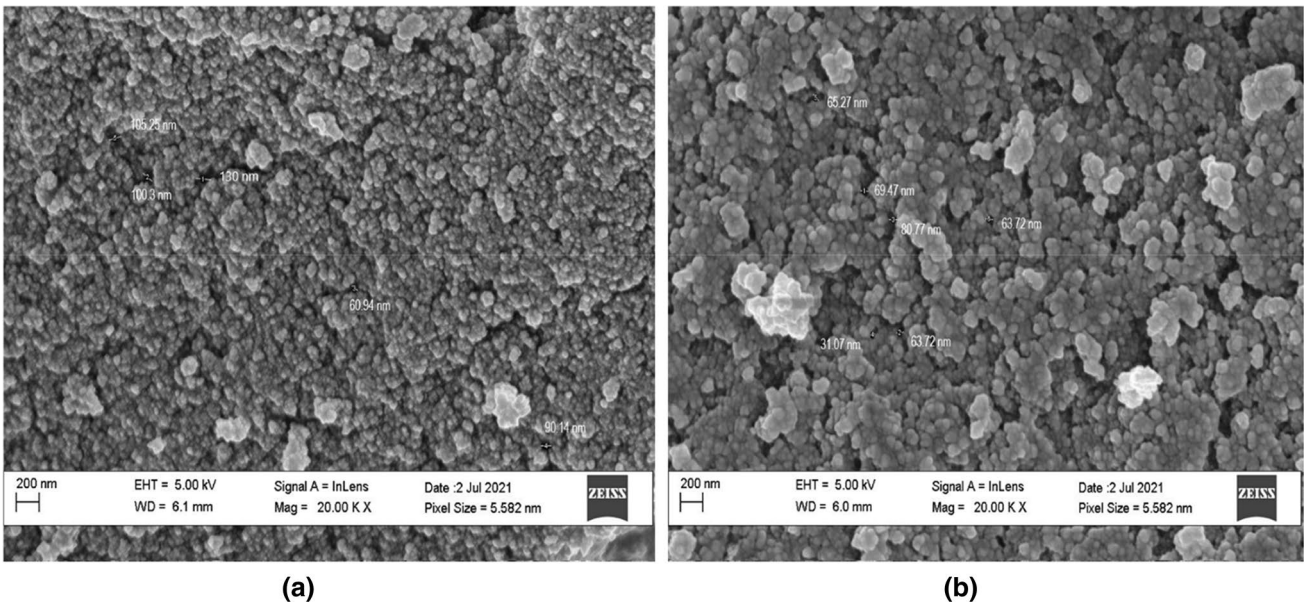

Fig. 3 SEM images of Amberchrom XAD-4 **a** before and **b** after impregnation with D2EHPA

unmodified resin's varying pore sizes, ranging from 60 to 130 nm. In Fig. 3b a significant decrease in pore size can be observed, indicating the uptake of D2EHPA within the resin structure.

Adsorption studies

Synthetic solutions were prepared for the batch sorption experiments. The influence of several physicochemical parameters (pH, adsorbent dosage, contact time, and initial scandium ion concentration) on Sc^{3+} adsorption onto D2EHPA impregnated Amberlite XAD-4 resin was evaluated.

Adsorbent dosage

The effect which sorbent mass has on the sorption of Sc^{3+} was evaluated, as illustrated in Fig. 4. The resin mass varied from 0.1 g to 3.0 g. A 4.0 mg dm^{-3} Sc^{3+} solution was used. The sorption of Sc^{3+} increased from 56 and 91%, with increasing sorbent dosage. This increase in % sorption can be ascribed to the increase in the available sites for metal ion adsorption, leading to increased sorption of metal ions. It was observed that by increasing the amount of adsorbent from 0.1 g to 1.0 g, the % sorption remained constant with further increases up to 3.0 g. This can be a result of sorption sites overlapping, as opposed to the overfilling of adsorbent particles. Based on these results, the optimal sorbent mass used for Sc^{3+} sorption studies was 1.0 g.

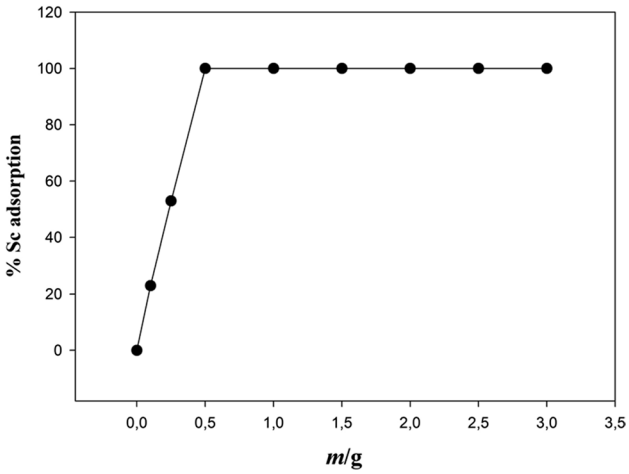

Fig. 4 Effect of sorbent dosage

Effect of pH

The pH of a solution is an essential variable in the adsorption or extraction of metal ions onto specific sorbents or supports. Evaluating the effect of pH on the sorption process could give a better understanding of the mechanism involved in the uptake of the metal ions onto the surface of the resin. The metal ions in aqueous solutions are inclined to exchange with H^+ ions from the extractant impregnated onto the adsorbent. The effect of the sorption behavior of scandium onto the D2EHPA impregnated resin can thus be explained, based on the extraction behavior of solvent extraction using D2EHPA. The influence of acidity in

terms of pH, on the sorption of Sc^{3+} in a pH range of 2 to 9, was investigated.

Scandium mostly exists as Sc^{3+} in an aqueous acidic solution. The Sc^{3+} extraction using D2EHPA is governed by the cation exchange mechanism at low acidity, according to the following equation [32]:

$$Sc^{3+}(aq) + 3\{HL\}(org) = \{ScL_3\}_{(org)} + 3H^{+}(aq) \quad (2)$$

In Fig. 5a, b, sorption is highest at pH = 2, with a maximum capacity of 0.050 mg g^{-1}. This result is in agreement with a study done by P.A Nikolaychuk [12]. However, with an increase in pH, the % Sc^{3+} sorption showed a decreasing trend up to pH = 5, before an increase at pH = 6. Scandium can be hydrolysed to $ScOH^{2+}$ (aq), $Sc(OH)_2{}^{+}$ (aq), or $Sc(OH)_4{}^{-}$ (aq) with an increase in solution pH [29]. The increased scandium sorption observed at pH = 6 could be ascribed to the precipitation of $Sc(OH)_3$ (s), based on the Eh–pH and speciation diagrams of a study by [12]. With percentage sorption of 100% at a pH of 2, quantitative sorption of scandium is seemly affected by solution pH.

The distribution coefficients for the different sorption pH solutions were determined, as shown in Table 1. The high K_d value observed at pH = 2 confirms the affinity of the resin with Sc^{3+} at the specified pH.

The predominance of scandium species (Sc^{3+}, $ScCl_2{}^{+}$, and $Sc(OH)_2{}^{-}$) in the solution is impacted by the pH of the respective solution. Figure 5 indicates that the adsorption of scandium is the highest at pH = 2. These results compare to data from a study done by [12], where an increase in scandium adsorption was observed between pH = 0 and pH = 2.

Table 1 Sorption efficiency, sorption capacity and K_d for Sc with varying pH

pH	Initial conc/mg dm^{-3}	Equilibrium conc/mg dm^{-3}	% Sorption	q_e/mg g^{-1}	K_d
2	2.0	0.000	100.00	0.0500	> 1 000 000
3	2.0	0.145	92.75	0.0464	1279
4	2.0	0.175	91.25	0.0456	1042
5	2.0	0.140	93.00	0.0465	1329
6	2.0	0.005	99.77	0.0499	39,900
7	2.0	0.020	99.00	0.0495	9900
8	2.0	0.030	98.50	0.0493	6567
9	2.0	0.064	96.80	0.0484	3025

Sorption kinetics

Sorption kinetics is an essential parameter in the sorption process as it aids in determining the contact time required for maximum adsorption. Several mathematical models describe adsorption data; they can be categorized as adsorption reaction models and adsorption diffusion models [25]. The pseudo-first-order and pseudo-second-order models were used to describe reaction kinetics, while the Weber Morris model was used to describe the reaction diffusion.

Reaction kinetics

To evaluate the effect of contact time on the sorption of Sc^{3+} ions, the studies were performed at a pH = 2 and sampled at different times, ranging from 10 min to 24 h. The sorption of Sc^{3+} ions increases steadily up to 24 h. The sorption

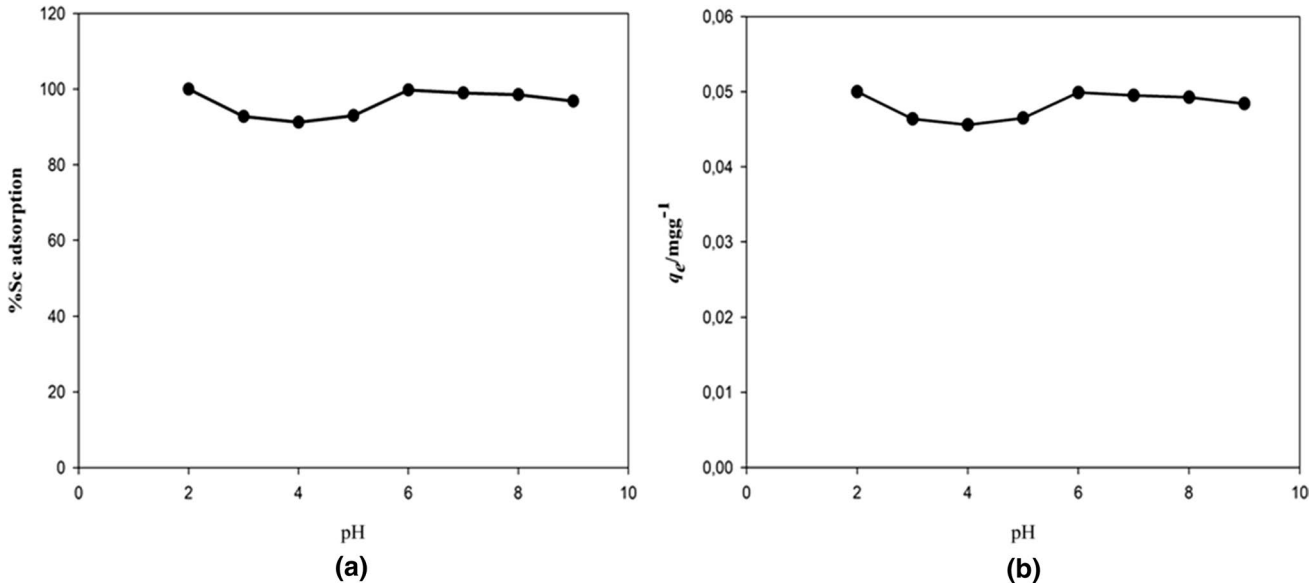

Fig. 5 **a** Scandium sorption efficiency as a function of pH and **b** sorption capacity of scandium as a function of pH

efficiency of Sc^{3+} increased by only 7% from 4 to 24 h, with a maximum capacity of 0.034 mg g^{-1}. The results are shown in Fig. 6a, b. A sufficient contact time of 4 h was selected for sorption equilibrium to be attained; 93% of Sc^{3+} was sorbed.

The pseudo-first-order and pseudo-second-order models were applied to analyze the sorption data for scandium. The plots are shown in Fig. 7a, b.

The integrated form of the pseudo-first-order model used is illustrated as follows:

$$\log (q_e - q_t) = \log q_e \frac{k_1 t}{2.303} \quad (3)$$

where q_e (mg/g) and q_t (mg/g) is the amount of metal sorbed at equilibrium time and the amount of metal sorbed at any time, respectively. The pseudo-first-order rate constant, k_1 (min^{-1}), can be obtained from the slope of the linear plot of log (q_e-q_t) against time (t).

The integrated pseudo-second-order model used is illustrated as follows:

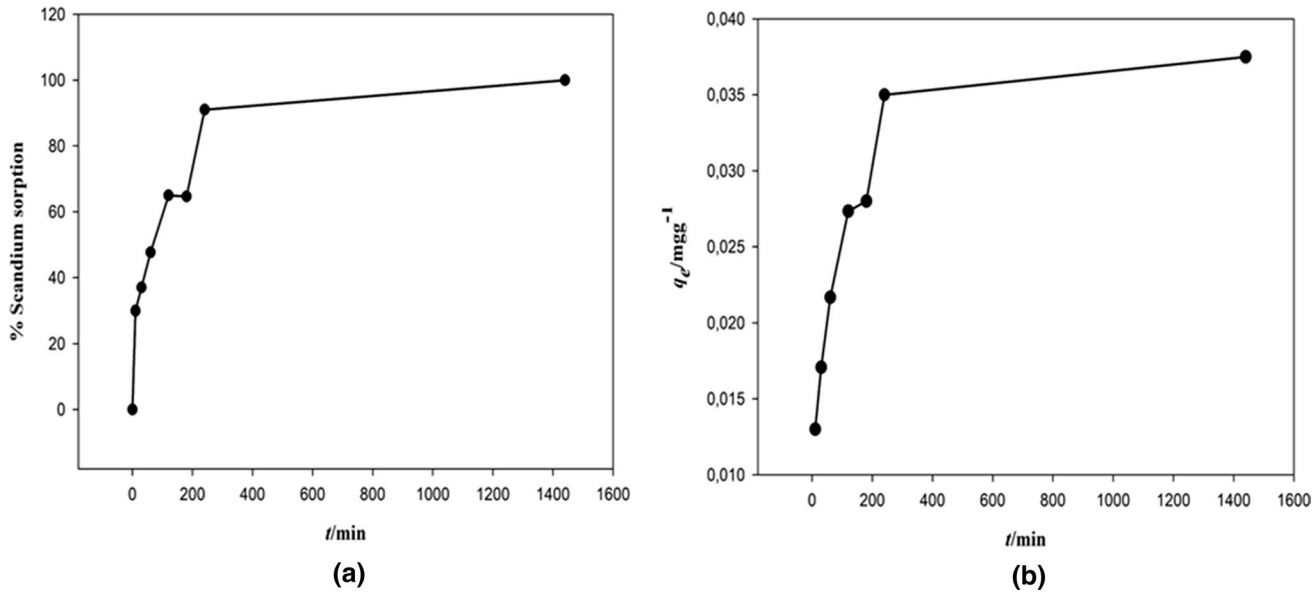

Fig. 6 **a** Effect of contact time on scandium sorption efficiency and **b** scandium sorption capacity over time

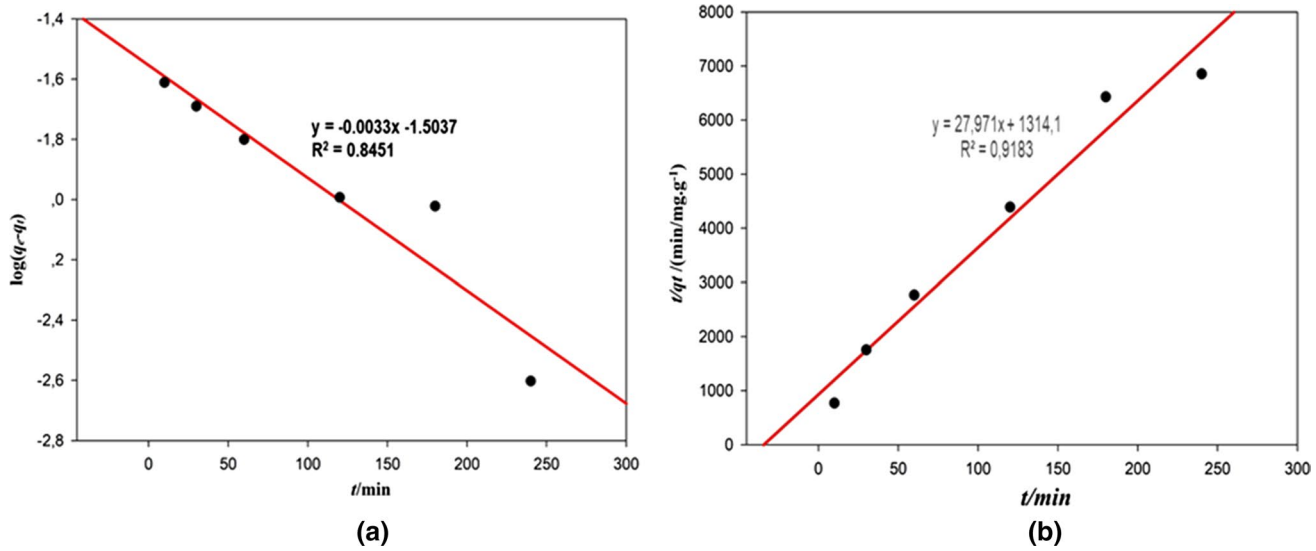

Fig. 7 **a** Pseudo-first-order plot for scandium sorption and **b** pseudo-second-order plot for scandium sorption

$$\frac{t}{q_t} = \frac{1}{k_2 qe^2} + \frac{t}{q_e} \quad (4)$$

where k_2 (g/mg min) and q_e can be obtained from the plot between t/q_e versus t [25].

From Fig. 7a, the first-order rate constant was determined from the slope of the curve, and the sorption capacity was determined from the intercept. The pseudo-second-order rate constant and sorption capacity were calculated from the intercept and slope, respectively, in Fig. 7b. A summary of the kinetics parameters for both the pseudo-first-order and pseudo-second-order models is presented in Table 2.

The correlation coefficients for pseudo-first-order and pseudo-second-order models were 0.8451 and 0.9183, respectively. The pseudo-second-order graph has a higher correlation between the experimental parameters, suggesting that the scandium data is best modelled by the pseudo-second-order kinetics. A theoretically predicted adsorption capacity, compared to the experimental value, confirms that the pseudo-second-order kinetics model is the better fit and that the sorption is occurring via a chemical process [25, 26].

Diffusion kinetics

The Weber Morris diffusion model was used to describe the sorption of scandium onto D2EHPA impregnated resin. This model is based on the assumption that the overall sorption process is controlled by either one or a combination of factors, for example, film diffusion, pore diffusion, surface diffusion, and sorption onto the adsorbent pore surface [27]. The equation for this model is expressed as follows:

$$q = kt^{1/2} + I \quad (5)$$

where k is the diffusion rate parameter (mg dm^{-3} s$^{-1/2}$), and the value of I can be calculated from the intercept from the plot of q versus $t^{1/2}$ [34]. The Weber Morris plot for scandium is presented in Fig. 8.

Intra-particle diffusion is normally considered the rate-controlling step when the linear plot of q_e against $t^{1/2}$ passes through the origin. The plot of q_e against $t^{1/2}$ did not pass through the origin, nor did it produce a straight line, suggesting intra-particle diffusion was not the only diffusion mechanism involved. It may also indicate that sorption diffusion kinetics may be controlled by film diffusion and pore diffusion. Multi-linearity suggests that both diffusion mechanisms are present and can thus control the sorption process. Multi-linearity also implies that varying pore sizes influenced the diffusion of Sc^{3+} ions through the resin structure, as was confirmed by the SEM images of the impregnated resin.

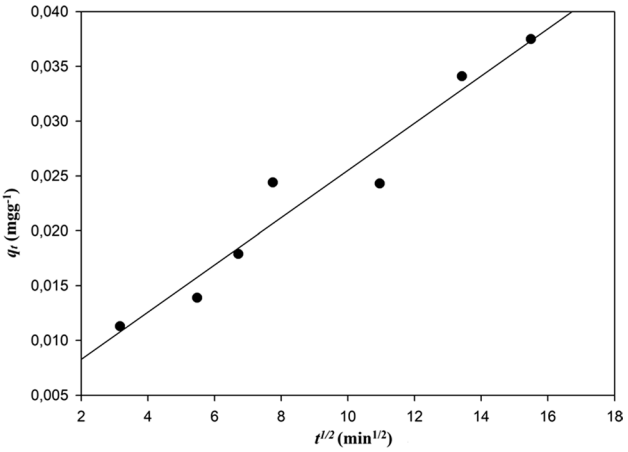

Fig. 8 **a** Weber Morris diffusion kinetics plot for scandium sorption and **b** interparticle diffusion kinetics for scandium removal using impregnated resin

Sorption isotherms

Adsorption isotherms are valuable and essential to understanding the relationship between metal ions (sorbate) and sorbent during an adsorption process. This study's experimental equilibrium data were subjected to four adsorption equilibrium isotherm models (Langmuir, Freundlich, Temkin, and Dubinin-Radushkevich).

The effect of initial metal ion concentration on the sorption of Sc^{3+} was evaluated using 1 g of impregnated resin and a solution having a pH = 2. The results are illustrated in Fig. 9 and shown in Table 3. As shown in Fig. 9a a sorption efficiency of 100% was achived at a concentration of 1.0 mg dm^{-3}. The sorption capacity had a linear increase over the concentration range, with no plateau reached (Fig. 9b).

The experimental data were subjected to the four isotherm models. Of the four isotherms, the Langmuir isotherm provided the best fit for the experimental data, with a high linear regression coefficient of $R^2 = 0.9934$ (Fig. 10a). The other three isotherms (Freundlich, Temkin, and Dubinin-Radushkevich), had very low regression coefficients and

Table 2 Kinetic parameters for Sc sorption on impregnated resin

	Pseudo first order			Pseudo second order		
q_e/mg g^{-1}	R^2	q_e/mg g^{-1}	k_1/min^{-1}	R^2	q_e/mg g^{-1}	k_2/g mg^{-1} min^{-1}
0.0341	0.8451	0.0313	0.0076	0.9183	0.0358	0.5938

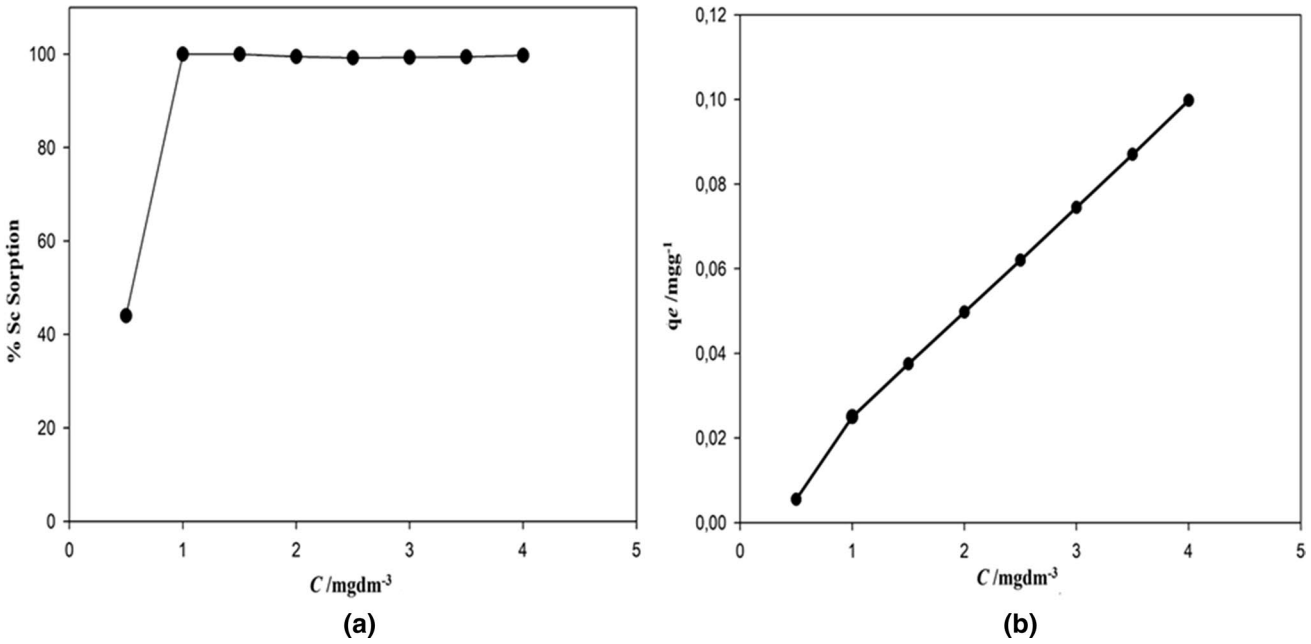

Fig. 9 **a** Scandium sorption efficiency with varying initial concentration and **b** sorption capacity as function of concentration

Table 3 Sc sorption with varying initial concentration

Initial conc/ mg dm^{-3}	Equilibrium conc/mg dm^{-3}	q_e/mg g^{-1}	% Sorption	K_d
0.50	0.28	0.1573	44	78.57
1.0	0.00	0.1677	100	> 900 000
1.5	0.00	0.1677	100	> 900 000
2.0	0.01	0.1663	99.5	19 900
2.5	0.02	0.1660	99.2	12 400
3.0	0.02	0.1660	99.3	14 900
3.5	0.02	0.1660	99.4	17 400
4.0	0.01	0.1663	99.8	39 900

their calculated capacities correlated poorly with the experimental value. The mean sorption energy (E) obtained from the Dubinin-Radushkevich plot was 158 kJ mol^{-1}, which signifies chemisorption as the sorption mechanism involved in Sc sorption, using the impregnated resin.

The linearized form of the Langmuir isotherm equation is expressed as follows:

$$\frac{C_e}{q_e} = \frac{\alpha_L C_e}{K_L} + \frac{1}{K_L} \tag{6}$$

where K_L and α_L are the equilibrium constants of the Langmuir equation. The plot of C_e/q_e against C_e yields a straight line with a slope, α_L/K_L, and intercept $1/K_L$ [39].

The essential feature of the Langmuir isotherm can be expressed in terms of a separation factor, calculated from the following equation [36]:

$$R_L = \frac{1}{\left(1 + K_L C_o\right)} \tag{7}$$

The value of R_L was calculated to be 6.8×10^{-3}. It falls within the range of 0–1 at optimum pH, confirming the favourable adsorption of Sc^{3+} ions onto the impregnated resin [35].

The logarithmic form of the Freundlich isotherm equation is expressed as follows:

$$\log q_e = \log K_f + \frac{1}{n} \log C_e \tag{8}$$

where K_f (mg/g) is the binding energy constant reflecting the affinity of the adsorbents with the metal ions where $\frac{1}{n}$ is the constant indicating the intensity of the adsorption [25].

The linear form of the Temkin isotherm is expressed as follows:

$$q_e = \frac{R_t}{b}(\ln K_T + \ln C_e) \tag{9}$$

where b is the Temkin constant, related to the heat of sorption (J mol^{-1}), and K_T is the Temkin isotherm constant (dm^3 g^{-1}) [39].

The Dubinin–Radushkevich isotherm is expressed as follows:

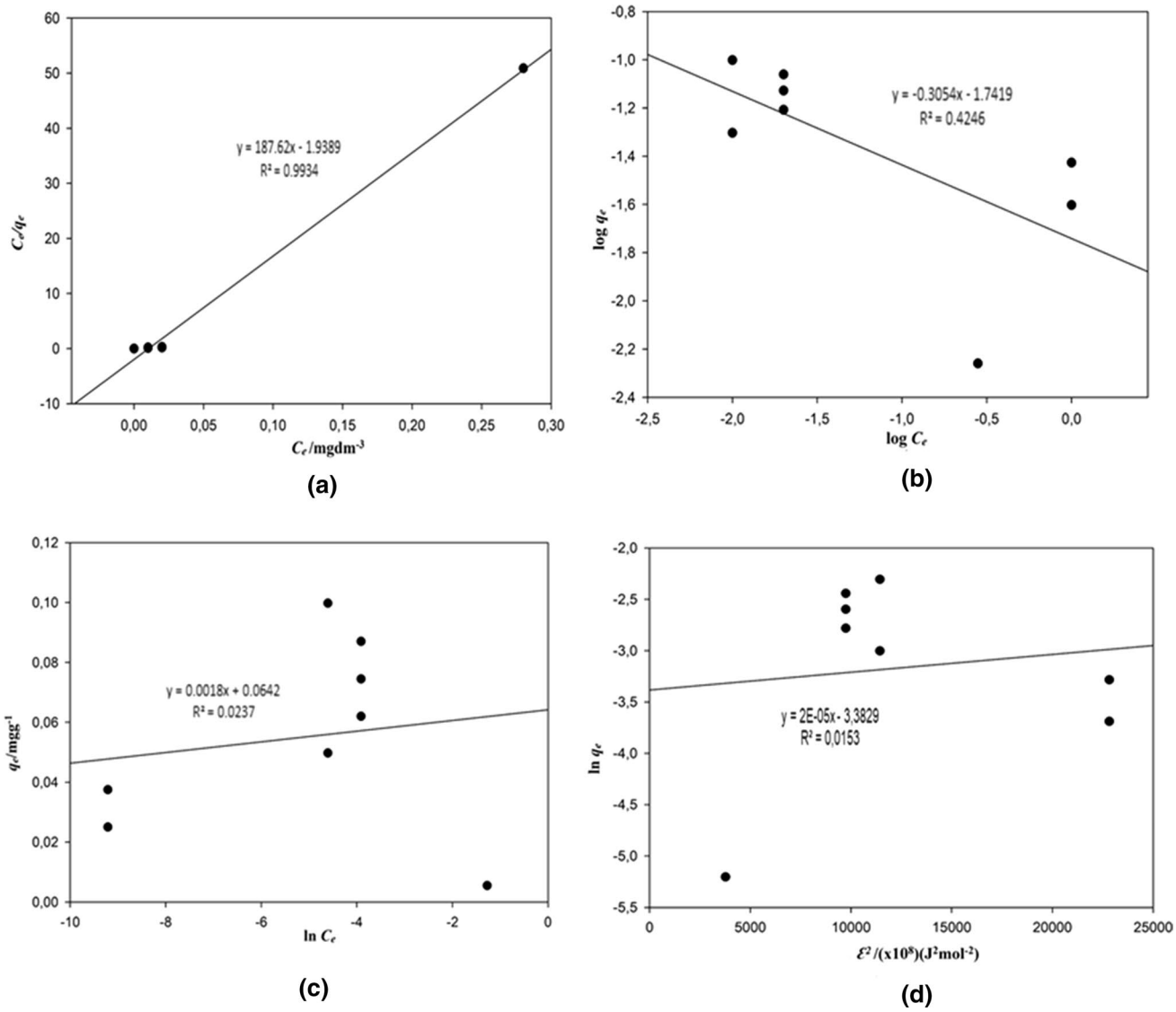

Fig. 10 **a** Langmuir isotherm, **b** Freundlich isotherm, **c** Temkin isotherm, and **d** Dubinin-Radushkevic

$$\ln q_e = \ln q_m \beta \varepsilon^2$$

where $\mathcal{E} = RT \ln(1 + 1/C_e)$ is the Polanyi potential, R is gas constant (8.31 J mol^{-1} k^{-1}), T is absolute temperature, and C_e is the equilibrium concentration. β is the Dubinin–Radushkevich constant and q_m is the sorption capacity.

The mean sorption energy (E) obtained from the Dubinin–Radushkevich plot is applied so as to differentiate between the chemical and physical sorption of metal ions. It was calculated as follows [40]:

$$E = \frac{1}{\sqrt{2\beta}} \tag{10}$$

When the magnitude of E in the range 8—16 kJ mol^{-1} signifies chemisorption as sorption mechanism, whereas $E < 8$ kJ mol^{-1} suggests physisorption [40].

Table 4 Characteristic parameters of Sc sorption isotherms

Isotherm	Correlation coefficient	Parameters
Langmuir	0.9934	$q_m = 0.00532$ mg g^{-1} $K_L = 96.757$ dm^3 mg^{-1}
Temkin	0.0237	$RT/b = 0.0018$ J mol^{-1} $K_T = 3.1 \times 10^{12}$
Freundlich	0.4246	$K_F = 0.4949$ mg g^{-1} $n = 1.7419$
Dubinin-Radushkevich	0.0153	$X_m = 29.456$ mg g^{-1} $\beta = 2 \times 10^{-5}$ mol^2 kJ^{-2} $E = 158.1$ kJ mol^{-1}

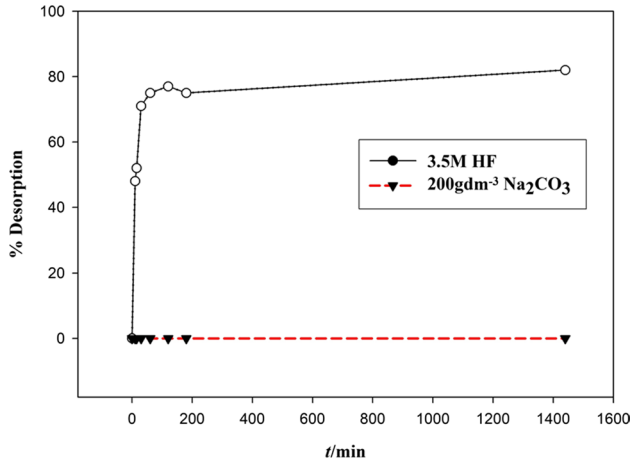

Fig. 11 Desorption of scandium ions as a function of time

A summary of the characteristic parameters for each of the four isotherms is presented in Table 4.

Desorption studies

The desorption of scandium from the XAD-4-D2EHPA resin was carried out under static conditions using two desorption solutions. Desorption solutions of the following concentrations were used: 200 g dm^{-3} Na_2CO_3 and 3.5 M HF. A mass of approximately 1 g of resin for each experiment was used. The results of the scandium desorption from the XAD-4-D2EHPA resin are shown in Fig. 11.

From the results illustrated in Fig. 11, when 3.5 M HF was used as a desorption solution, approximately 80% of the scandium was extracted from the XAD-4-D2EHPA resin under static conditions. The Na_2CO_3 solution showed very low to no desorption characteristics, which is contradictory to results that were established by Ivanov et al. [36]. The desorption results obtained from a 3.5 M HF desorption solution are in agreement with the literature.

Conclusion

Equilibrium and kinetic studies were conducted to evaluate the adsorption of scandium from aqueous solutions using di(2-ethylhexyl)phosphoric acid (D2EHPA) impregnated onto Amberlite XAD-4. The physical interaction of D2EHPA with the Amberlite XAD-4 resin was demonstrated using FT-IR. The suitable equilibrium time for this study was 4 h, with a scandium removal of 93%. The solution pH significantly affected the scandium(III) adsorption, with maximum adsorption at a pH of 2. The Langmuir and Freundlich isotherms were used to analyze the equilibrium adsorption data. The characteristic parameters and related relative correlation coefficients were determined for each isotherm. The Langmuir isotherm demonstrated a good correlation compared to the Freundlich model. The sorption kinetics data agree with the pseudo-second-order model more than the pseudo-first-order model, with a theoretically predicted adsorption capacity closely corresponding to the experimental value. This further indicates that a chemisorption process controls the rate of reaction. An adsorption capacity of 0.035 mg Sc per gram of impregnated resin was achieved. It can be concluded that the scandium can successfully be removed from aqueous solutions using the Amberlite XAD-4-D2EHPA impregnated resin and that HF is a suitable eluant to desorb scandium from the surface of the modified resin with an 80% recovery.

The results obtained from this study are reasonably promising and applicable for the extraction and recovery of scandium, because of the expected future demand for scandium, especially with its application in the new generation of solid oxide fuel cells.

Experimental

Di(2-ethylhexyl)phosphoric acid (D2EHPA) (> 95%) was purchased from Sigma Aldrich, and Amberlite XAD-4 resin was purchased from Industrial Analytical. The HCl and HNO_3 acids, and NaOH were of analytical grade and used without further purification. Deionized water was used for all the preparations.

All pH measurements were taken using a digital pH meter (Basic 20 + CRISON), with a glass electrode, which was calibrated with buffer solutions. An automatic mechanical shaker (Labotec model 262) with speed control was used for the impregnation process and all the batch equilibrium studies. The Spectro ARCOS ICP-OES spectrometer was used to measure all metal ion concentrations. A Spectrum, 2 FT-IR Spectrometer manufactured by Perkin-Elmer, was used to record the FT-IR spectra of the unmodified and modified (impregnated) Amberlite XAD-4-D2EHPA resin in the range of 400 – 4000 cm^{-1}. A Zeiss MERLIN Field Emission Scanning Electron Microscope was used to analyze the surface morphology of the resin, pre- and post-impregnation.

Preparation of stock solutions

A 10 mg dm^{-3} scandium stock solution was prepared in 500 cm^3 of deionized water, used for all the batch experiments. The calibration standards in the concentration range of 0.1—10.0 mg dm^{-3} were prepared by serial dilution of

a stock solution that was prepared by diluting 12.5 cm^3 of a 1000 mg dm^{-3} analytical grade ICP standard in 250 cm^3 dilute nitric acid.

Conditioning and impregnation of Amberlite XAD-4 resin

The Amberlite XAD-4 was successively pre-treated with 50 cm^3 of 2 M HNO_3, 50 cm^3 2 M NaOH, followed by deionized water until it was neutralized (pH = 6.5 to 7) to remove impurities. The resin was then dried at 60 ℃ overnight and stored in a polyethylene bottle before use. Following the pre-treatment of the Amberlite XAD-4 resin, a desired amount of D2EHPA was dissolved in 65 cm^3 of diethyl ether. 10 g of the pre-treated resin was added, and the mixture was then placed on a mechanical shaker for 2 h. The mixture was then filtered under vacuum, the resins were subsequently placed overnight in a vacuum oven at 40 °C to remove the solvent.

The loading capacity of the resin was determined by using a pre-determined mass of resin placed in contact with ethanol. The solution was then titrated with 0.1 M NaOH until a light pink colour change was reached (endpoint). FT-IR spectroscopy was used to establish the interaction between the extractant (D2EHPA) and the Amberlite XAD-4 resin.

Procedure for the adsorption studies

The effect of pH, adsorbent dosage, initial metal ion concentration and contact time were evaluated. A brief methodology is provided below.

Effect of pH

The extent of scandium sorption at varying pH values was assessed in the batch experiments. Samples were prepared by mixing precisely 1 g of resin with 25 cm^3 of 2 mg dm^{-3} scandium (III) ion solutions at different pH values; they were adjusted with HCl and NaOH over a period of 4 h.

Effect of adsorbent dosage

The optimum adsorbent dosage was assessed. Samples were prepared by mixing different masses (ranging from 0.1 g—3.0 g) of impregnated resin with 25 cm^3 of 4.0 mg dm^{-3} scandium (III) ion solutions and shaken for 4 h on an automatic orbital shaker.

Effect of initial metal ion concentration

The effect of initial scandium concentration was assessed using scandium(III) solutions with initial concentrations varying between 0.5 and 4 mg dm^{-3}. All the batch experiments were conducted using the Labotec model 263 automatic mechanical shaker at an ambient temperature for 4 h. The Langmuir and Freundlich models were used to model the equilibrium data.

Effect of contact time

The effect of contact time was studied by mixing 1 g of resin with 25 cm^3 of 1.5 mg dm^{-3} scandium(III) ion solutions at different contact times (10, 30, 60, 120, 180, 240 min and 24 h).

Adsorption isotherms and kinetics procedure

Adsorption isotherms were investigated by mixing 1 g of resin with 25 cm^3 of 1.5 mg dm^{-3} scandium(III) solution at a pH = 2. The solutions were placed on a shaker for 4 h at 150 rpm, with samples. The two-parameter isotherm models, Langmuir, Freundlich, Temkin, and Dubinin-Radushkevich, were used to analyze the equilibrium data of scandium(III) adsorption on the impregnated resin. The rate of adsorption was evaluated over 24 h, with samples taken at predetermined time intervals and scandium concentrations determined by ICP-OES.

Acknowledgements The authors wish to thank the Department of Chemistry, Cape Peninsula University of Technology, and especially the staff of the Instrumentation laboratory, Cape Town Campus. The authors would also wish to acknowledge the CPUT URF for financial support of this work. This research did not receive any specific grant from funding agencies in the public, commercial, or not-for-profit sectors.

References

1. Li G, Ye Q, Deng B, Luo J, Rao M, Peng Z, Jiang T (2018) Hydrometallurgy 176:62
2. Dehabadi M, Legin E, Legin A, Yaghmaei S, Nechaev A, Babain V, Kirsanov D (2021) Sens Actuators, B Chem 348:130699
3. Junior AB, Espinosa DCR, Vaughan J, Tenório JAS (2021) Miner Eng 172:107148
4. Jeong D, Kim J, Kwon O, Lim C, Sengodan S, Shin J, Kim G (2018) Appl Sci 8:2217
5. Greb L (2018) Chem Eur J 24:17881

6. Giret S, Hu Y, Masoumifard N, Boulanger JF, Juère E, Kleitz F, Larivière D (2018) ACS Appl Mater Interf 10:448
7. Sharaf M, Yoshida W, Kubota F, Goto M (2019) J Chem Eng Jpn 52:49
8. Zhang N, Li HX, Liu XM (2016) Rare Met 35:887
9. Dong Z, Deblonde G, Middleton A, Hu D, Dohnalkova A, Kovarik L, Qafoku O, Shutthanandan V, Jin H, Hsu-Kim H, Theaker N (2021) Environ Sci Technol 55:6320
10. Shi C, Jing Y, Xiao J, Wang X, Yao Y, Jia Y (2017) Sep Purif Technol 172:473
11. Van Nguyen N, Iizuka A, Shibata E, Nakamura T (2016) Hydrometallurgy 165:51
12. Nikolaychuk PA (2016) Reg Geosyst 37:70
13. Kumar S, Jain S (2013) J Chem 2013:957647
14. Hajmohammadi H, Jafari AH, Nasab ME (2020) Trans Nonferrous Met Soc China 30:3103
15. Zhu X, Li W, Tang S, Zeng M, Bai P, Chen L (2017) Chemosphere 175:365
16. Makanyire T, Sanchez-Segado S, Jha A (2016) Adv Manufact 4:33
17. Batra S, Awasthi A, Iqbal M, Datta D (2022) Rev Chem Eng 38:209
18. Cortina JL, Warshawsky A (2021). In: Marinsky JA, Marcus J (eds) Ion exchange and solvent extraction, 1st edn. CRC Press, Boca Raton
19. Surya AKGV, Vithya J, Rajarajan S, Kumar R (2021) Radiochim Acta 109:215
20. Kalal HS, Khanchi AR, Nejatlabbaf M, Almasian MR, Saberyan K, Taghiof M (2017) Adv Environ Res 6:301
21. Bao S, Tang Y, Zhang Y, Liang L (2016) Chem Eng Technol 39:1377
22. Tetgure SR, Choudhary BC, Garole DJ, Borse AU, Sawant AD, Prasad S (2017) Microchem J 130:442
23. Tang Y, Bao S, Zhang Y, Liang L (2017) React Funct Polym 113:50
24. Chen JH, Chang YH, Hsu KC, Lin JC (2021) Chem Eng Technol 44:2257
25. Asuquo E, Martin A, Nzerem P, Siperstein F, Fan X (2017) J Environ Chem Eng 5:679
26. Zhu Q, Moggridge GD, D'Agostino C (2016) Chem Eng J 306:1223
27. Hosseini-Bandegharaei A, Allahabadi A, Rahmani-Sani A, Rastegar A, Khamirchi R, Mehrpouyan M, Hekmat-Shoar R, Pajohankia Z (2016) J Radioanal Nuclear Chem 309:761
28. Mineral Commodaties Summaries (2022) US Geological Survey, Reston, VA. https://www.usgs.gov. Accessed 11 June 2022
29. Wang L, Wang P, Chen WQ, Wang QQ, Lu HS (2020) J Clean Prod 270:122464
30. Longo S, Cellura M, Guarino F, Brunaccini G, Ferraro M (2019) Sci Total Environ 685:59
31. Li XY, Ge JP, Chen WQ, Wang P (2019) Resour Conserv Recycl 145:322
32. Das S, Behera SS, Murmu BM, Mohapatra RK, Mandal D, Samantray R, Parhi PK, Senanayake G (2018) Sep Purif Technol 202:248
33. Yuksekdag A, Kose-Mutlu B, Siddiqui AF, Wiesner MR, Koyuncu I (2022) Chemosphere 293:133620
34. Wang M, Zhou X, Liu Y, Xu H, Wu Y, Zhou L (2020) Appl Geochem 119:104639
35. Zhou J, Ma S, Chen Y, Ning S, Wei Y, Fujita T (2021) Hydrometallurgy 204:105724
36. Ivanov N, Abilmagzhanov A, Shokobayev N, Adelbayev I, Nurtazina A (2020) Proc Natl Acad Sci Repub Kaz, Ser Geol Tech Sci 4:156
37. Wang W, Pranolo Y, Cheng CY (2013) Sep Purif Technol 108:96
38. Bordean DM, Cojocariu A, Horablaga M, Cojocariu L, Alda S, Nica D, Alda L, Borozan AB (2013) Int Multidiscip Sci GeoConference: SGEM 1:865
39. Ayawei N, Ebelegi AN, Wankasi D (2017) J Chem 2017:3039817
40. Wang J, Guo X (2020) Chemosphere 258:127279